Advanced Journal of Chemistry, Section A

Journal homepage: www.ajchem-a.com

Original Research Article

Design, Synthesis, Molecular Docking, and Cytotoxic Evaluation of Novel Acridine-Based Aminoacetamide Derivatives as Potential Acetylcholinesterase Inhibitors

Joel Mart E., Ronald Darwin Chellappan*

Department of Pharmacology, School of Pharmaceutical Sciences, Vels Institute of Science, Technology and Advanced Studies (VISTAS), Chennai-600117, Tamil Nadu, India

ARTICLEINFO

Article history

Submitted: 2025-09-11
Revised: 2025-11-19
Accepted: 2025-11-22
ID: AJCA-2509-1924
DOI: 10.48309/AJCA.2026.546506.1924

KEYWORDS

Acridine derivatives
Acetylcholinesterase inhibitors
Molecular docking
Cytotoxicity
Structure–activity relationship
In vitro cytotoxicity

ABSTRACT

A series of novel acridine-based aminoacetamide derivatives (AN1, AN8, BI7, AAM3, and AC1) were synthesized and structurally confirmed using FTIR, NMR, and LC–MS techniques. This study aimed to evaluate the compounds as potential acetylcholinesterase (AChE) inhibitors with anticancer activity. Molecular docking was performed using the AChE crystal structure (PDB ID: 4EY6) to predict ligand–enzyme interactions. All derivatives showed favorable binding affinities (–8.0 to –8.3 kcal/mol), indicating strong compatibility with the catalytic pocket. AC1 demonstrated the highest affinity (–8.3 kcal/mol), supported by hydrogen bonds with Gly437 and Arg434, along with π–π stacking with Trp441 and Trp754, while AN1 and AN8 exhibited stable poses through π–cation and hydrogen bonding interactions. The cytotoxic potential of the derivatives was assessed against SH-SY5Y neuroblastoma cells using the MTT assay. AC1 displayed the strongest antiproliferative effect (IC_{50} = 26.92 ± 0.57 µg/mL), surpassing the standard reference compound (IC_{50} = 92.67 ± 0.43 µg/mL). AN1 (IC_{50} = 47.74 ± 0.98 µg/mL) and AN8 (IC_{50} = 69.95 ± 0.49 µg/mL) showed moderate cytotoxicity, while BI7 and AAM3 were considerably less active (IC_{50} values > 277 µg/mL). A clear correlation was observed between docking affinity and experimental cytotoxicity, particularly for AC1 and AN1. Overall, AC1 emerged as the most promising derivative, highlighting the impact of structural modifications on anticancer activity. The combined computational and *in vitro* results support acridine-based aminoacetamide scaffolds as potential leads for anticancer drug development.

* Corresponding author: Darwin Chellappan, Ronald
✉ E-mail: ronaldpharma@gmail.com

GRAPHICAL ABSTRACT

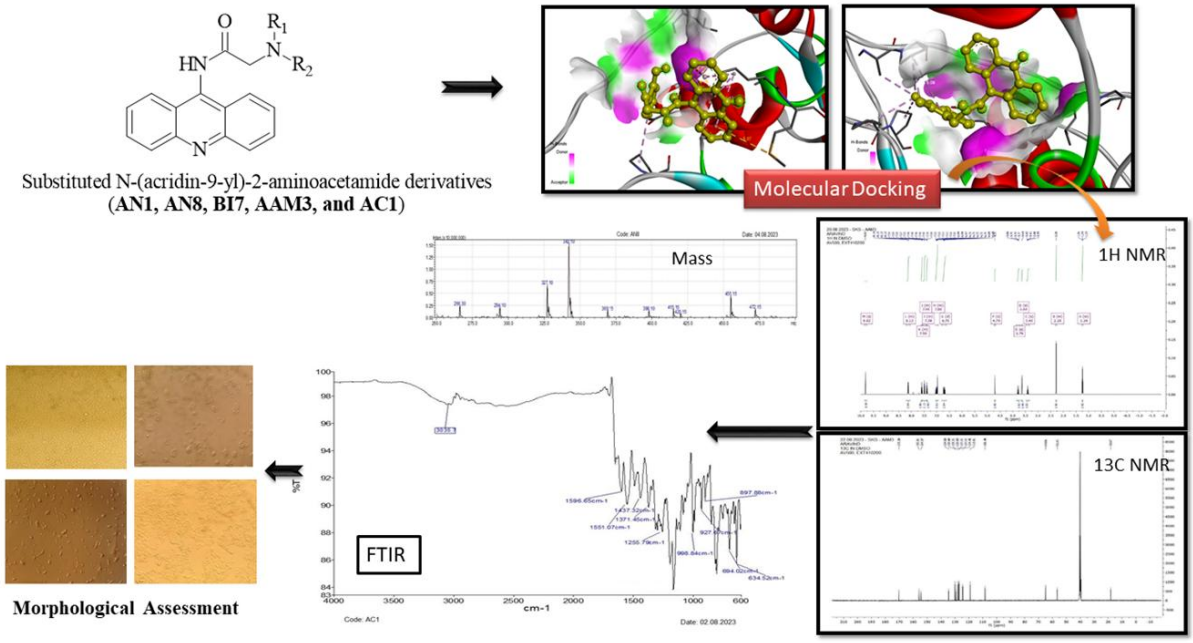

Introduction

The rational design, synthesis, and biological evaluation of heterocyclic compounds remain a cornerstone of modern medicinal chemistry because of their structural diversity and versatile pharmacological properties. Among the various heteroaromatic scaffolds, acridine has drawn considerable attention because of its unique planar tricyclic aromatic framework, which readily interacts with nucleic acids, enzymes, and receptor proteins. Acridine derivatives have been extensively investigated for their antimicrobial, antiviral, antimalarial, anti-inflammatory, and anticancer activities and have several reaching clinical use [1–3]. For example, amsacrine, an acridine-based anticancer drug, exerts its therapeutic effects through DNA intercalation and inhibition of topoisomerase II, whereas acriflavine has been employed as an antiseptic and more recently as an anticancer agent because of its ability to suppress HIF-1 signaling. These examples highlight the pharmacological versatility and therapeutic potential of the acridine nucleus.

Due to its planar aromatic framework and modifiable substituents, acridine is an attractive platform for drug discovery. Its flat aromatic system facilitates DNA intercalation, enabling disruption of nucleic acid functions, whereas its electron-rich heteroatoms and substitutable positions allow fine-tuning of interactions with enzymatic and protein targets. Consequently, acridine derivatives are often described as "privileged scaffolds, " which are capable of engaging multiple biological pathways, making them highly adaptable for the development of targeted therapeutics [4–6]. Given these therapeutic implications, the next step was to explore acridine derivatives as AChE inhibitors with anticancer potential.

One of the emerging areas in which acridine derivatives have shown promise is the inhibition of AChE. AChE is a crucial enzyme in the CNS that

hydrolyzes the neurotransmitter acetylcholine, thereby concluding synaptic communication [7–9]. Dysfunctional regulation of AChE is involved in several neurological diseases, most notably Alzheimer's disease, where AChE inhibitors such as donepezil, rivastigmine, and galantamine remain the mainstay of symptomatic treatment [10–12]. In addition to neurodegeneration, AChE is increasingly associated with cancer biology. Overexpression of AChE has been reported in certain tumors, where it contributes to tumorigenesis, apoptotic regulation, and modulation of signaling pathways. This dual role makes AChE an intriguing therapeutic target, not only for neuroprotective interventions, but also for anticancer strategies. Recent studies have further emphasized the regulatory influence of AChE on tumor progression, apoptosis modulation, and cellular proliferation across several cancers, highlighting its relevance as a multifunctional therapeutic target. These findings underscore the need for continued exploration of dual AChE-inhibitory and anticancer scaffolds [13–18].

The drug discovery process for AChE inhibitors increasingly relies on an integrative approach that combines rational design, molecular docking, and experimental validation. Molecular docking serves as a computational tool to predict ligand–enzyme interactions, providing insight into the binding modes, hydrogen bonding, hydrophobic contacts, and π–π stacking interactions that stabilize drug–target complexes. By employing the crystal structures of AChE, such as PDB ID: 4EY6, docking simulations allow rapid screening and prioritization of candidate molecules prior to labor-intensive biological evaluation. Such structure-guided methods accelerate the identification of promising leads while reducing experimental costs [19–21].

Nevertheless, computational predictions must be complemented by experimental assays to assess the pharmacological relevance of designed molecules. Cytotoxicity assays are widely employed to establish the anticancer potential of novel compounds. Among the various *in vitro* models, SH-SY5Y neuroblastoma cells represent a versatile human-derived neuronal cell line that serves both as a model for neurobiology and as a cancer cell platform. Cytotoxicity is commonly evaluated using the MTT assay, a colorimetric technique that measures mitochondrial activity, as an indicator of cell viability. Together, docking and cytotoxicity testing provide a comprehensive evaluation of both molecular binding and functional cellular outcomes.

In this context, the present study reports the design, synthesis, molecular docking, and cytotoxicity evaluation of novel acridine-based aminoacetamide derivatives. The design rationale was to functionalize the acridine nucleus with diverse substituents at the aminoacetamide position, thereby exploring structure–activity relationships and optimizing the interactions with AChE. The synthesized derivatives *N*-(acridin-9-yl)-2-(phenylamino)acetamide(AN1), *N*-(acridin-9-yl)-2-((2-hydroxyphenyl)amino)acetamide (AN8), *N*-(acridin-9-yl)-2-(2,3-dimethyl-1H-indol-1-yl)acetamide (BI7), *N*-(acridin-9-yl)-2-(ethyl(o-tolyl)amino)acetamide (AAM3), and *N*-(acridin-9-yl)-2-(4-oxopiperidin-1-yl)acetamide (AC1), containing phenyl, hydroxylphenyl, indole, ethyl-tolyl, and oxopiperidine moieties, were chosen to probe variations in hydrophobicity, electronic effects, and hydrogen-bonding potential. These molecules were synthesized via nucleophilic substitution reactions and characterized using FTIR spectroscopy, NMR, and LC–MS to ensure structural confirmation and purity [22,23].

Molecular docking studies were conducted using AutoDock Vina to estimate binding affinities and visualize ligand–AChE interactions. Specific attention has been given to hydrogen bonds, π–π interactions with aromatic residues, and hydrophobic contacts in the active site gorge [19–21]. Docking scores were then compared with the experimental cytotoxicity data obtained from the

MTT assays against SH-SY5Y neuroblastoma cells. By correlating computational predictions with biological activity, this study sought to validate docking as a predictive tool for identifying effective AChE inhibitors with anticancer potential.

Overall, this study highlights the therapeutic significance of acridine-based scaffolds in targeting AChE for dual neuroprotective and anticancer applications. Among the tested derivatives, AC1 emerged as a promising candidate, demonstrating a strong docking affinity and notable cytotoxicity, thereby establishing its potential as a lead compound for further preclinical investigations.

Experimental

Synthesis of N-(acridin-9-yl)-2-chloroacetamide

Acridine-9-amine (1) 1.0 g (0.0011 mol, 1.0 equiv) was dissolved in acetone, and potassium carbonate 0.24 g (0.00179 mol, 1.5 equiv) was then added. After 15 min of stirring at ambient temperature, 0.242 g (0.00143 mol, 1.2 equivalents) of 2-chloroacetyl chloride was added, and the reaction mixture was agitated at room temperature for 4–12 h. The progress of the reaction was monitored by TLC using n-hexane:ethyl acetate (1:2 to 1:6) as the eluent, and spots were visulaized using a UV light chamber. The mixture was filtered, the filtrate was concentrated, and the resultant residue was processed.

Synthesis of substituted N-(acridin-9-yl)-2-aminoacetamide derivatives

DMF (40 mL) was added to the combination of substituted *N*-(acridin-9-yl)-2-chloroacetamide (3, 0.01 mol) and the corresponding substituted amine (4, 0.012 mol), followed by the addition of triethylamine (0.012 mol). The reaction mixture was refluxed for one hour at 150-155 ℃ until full consumption of the starting material, as determined by TLC. Upon completion of the reaction, the precipitate produced during cooling was filtered and recrystallized using ethanol to obtain the final compounds (**AN1**, **AN8**, **BI7, AAM3**, and **AC1**). A detailed reaction scheme is shown in Figure 1.

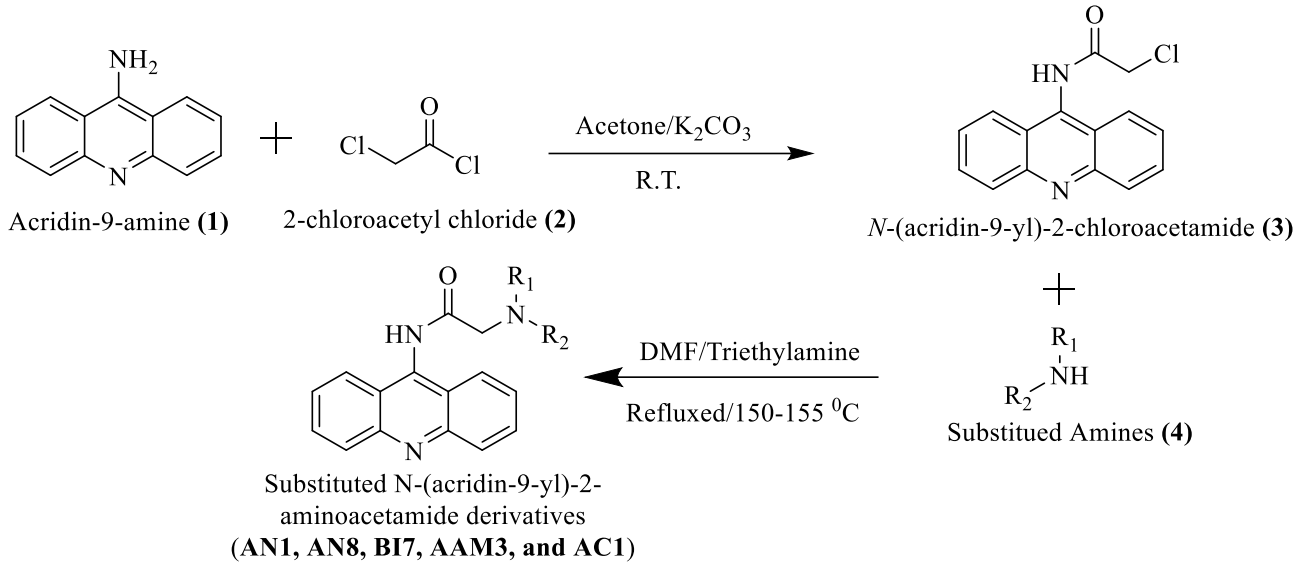

Figure 1. The proposed reaction scheme for the synthesis of substituted *N*-(acridin-9-yl)-2-aminoacetamide derivatives.

Characterization of synthesized compounds

The synthesized acridine derivatives (**AN1**, **AN8**, **BI7**, **AAM3**, and **AC1**) were characterized by melting point determination, thin-layer chromatography (Rf values), percentage yield, elemental analysis, and spectral methods, including FT-IR, ^{1}H-NMR, ^{13}C-NMR, and LC-MS [24,25]. The characterization spectra are provided in the Supplementary file, Tables S1-S4. Figure 2 illustrates the structures of the synthesized compounds.

*N-(acridin-9-yl)-2-(phenylamino)acetamide (**AN1**)*

Chemical formula: $C_{21}H_{17}N_3O$; M.P.: 122-125 °C; Rf: 0.98; % yield: 90. Molecular weight: 327.39 g/mol; m/z: 327.14 (100.0%), 328.14 (22.7%), 329.14 (2.5%), and 328.13 (1.1%). Elemental analysis (calculated): C, 77.04; H, 5.23; N, 12.84; and O = 4.89. ^{1}H-NMR (500 MHz, DMSO): δ 9.94 (s, 1H), 8.06 (dd, J = 7.5, 1.4 Hz, 2H), 7.73 (dd, J = 7.4, 1.5 Hz, 2H), 7.61 (td, J = 7.5, 1.5 Hz, 2H), 7.47 (td, J = 7.5, 1.5 Hz, 2H), 6.93 (d, J = 7.5 Hz, 2H), 6.73 (s, 1H), 6.38 (d, J = 7.5 Hz, 2H), 4.20 (s, 1H), 4.12 – 4.08 (m, 1H), and 3.81 (s, 1H). ^{13}C-NMR (101 MHz, DMSO): δ 166.02, 139.67, 135.45, 132.00, 129.05, 128.84, 128.14, 124.11, 120.86, 120.75, and 45.85. The FTIR spectra of AN1 exhibited a wide band at 3,344 cm^{-1}, indicative of N–H stretching in the amide functional group. Aromatic C–H stretching vibrations were observed at 3,080–3,000 cm^{-1}. A prominent peak at 1,678 cm^{-1} validated C=O stretching of the amide group, while supplementary bands at 1,644 and 1,609 cm^{-1} resulted from the aromatic C=C stretching. The peaks in the 1,515–1,456 cm^{-1} range were ascribed to C–N stretching and aromatic ring vibrations. The band at 1,214–1,095 cm^{-1} corresponds to C–N stretching of the aryl amine, whereas many strong peaks at 877–744 cm^{-1} show aromatic C–H out-of-plane bending, indicative of monosubstituted phenyl rings.

*N-(acridin-9-yl)-2-((2-hydroxyphenyl)amino)acetamide (**AN8**)*

Chemical formula: $C_{21}H_{17}N_3O_2$; M.P.: 140-143 °C; Rf value: 0.98; % yield: 90. Molecular weight: 343.39 g/mol; m/z: 343.13 (100.0%), 344.14 (22.7%), 345.14 (2.5%), and 344.13 (1.1%). Elemental analysis (calculated): C, 73.45; H, 4.99; N, 12.24; and O, 9.32. ^{1}H-NMR (500 MHz, DMSO) δ 9.95 (s, 1H), 9.84 (s, 2H), 8.26 – 7.90 (m, 2H), 7.95 – 7.85 (m, 1H), 7.73 (dd, J = 7.5, 1.4 Hz, 1H), 7.61 (td, J = 7.5, 1.6 Hz, 2H), 7.47 (td, J = 7.5, 1.5 Hz, 1H), 6.75 (s, 1H), 6.64 (td, J = 7.5, 1.5 Hz, 1H), 6.59 – 6.40 (m, 2H), 6.23 (dd, J = 7.5, 1.4 Hz, 1H), 6.23 (dd, J = 7.5, 1.4 Hz, 1H), 4.27 (d, J = 5.1 Hz, 2H), and 3.63 (s, 2H). ^{13}C-NMR (101 MHz, DMSO) δ 166.02, 139.67, 135.45, 132.00, 129.05, 128.84, 128.14, 124.11, 120.86, 120.75, and 45.85. The FTIR spectrum of AN8 exhibited a pronounced absorption at 3,195 cm^{-1}, signifying O–H stretching vibrations from the phenolic hydroxyl group. The peak at 2,986 cm^{-1} indicates C–H stretching. The pronounced band at 1,909 cm^{-1} was linked to the overtone and combination bands characteristic of aromatic systems. The amide C=O stretching was observed at 1,554 cm^{-1}, while the bands at 1,483–1,374 cm^{-1} corresponded to C–N and aromatic C=C stretching. Peaks within the range of 1,115–961 cm^{-1} corroborated the C–O stretching of the phenolic groups. Out-of-plane C–H bending vibrations were observed at 888–761 cm^{-1}, indicating aromatic substitution.

*N-(acridin-9-yl)-2-(2,3-dimethyl-1H-indol-1-yl)acetamide (**BI7**)*

Chemical formula: $C_{25}H_{21}N_3O$; M.P.: 179-183 °C; Rf value: 0.92; % yield: 80. Molecular weight: 379.46 g/mol; m/z: 379.17 (100.0%), 380.17 (27.0%), 381.18 (2.7%), 380.17 (1.1%). Elemental analysis (calculated): C, 79.13; H, 5.58; N, 11.07; and O = 4.22. ^{1}H-NMR (500 MHz, DMSO) δ 8.12 – 7.98 (m, 2H), 7.84 – 7.69 (m, 2H), 7.65 – 7.60 (m, 2H), 7.50 – 7.46 (m, 2H), 7.27 (s, 1H), 7.11

(s, 1H), 6.99 (s, 1H), 6.56 (d, J = 10.0 Hz, 2H), 5.26 (s, 1H), 5.01 (s, 1H), and 2.33 – 2.26 (m, 6H). ^{13}C-NMR (126 MHz, DMSO) δ 168.50, 156.63, 148.92, 148.40, 125.65, 122.36, 121.60, 109.59, 109.19, 106.93, 106.34, 102.56, 102.06, 54.16, 46.79, and 34.54. The FTIR spectrum of BI7 exhibited a wide band at 3,357 cm^{-1}, indicative of N–H stretching vibrations. The peaks at 3,073–2,732 cm^{-1} indicate aromatic and aliphatic C–H stretching, respectively. A prominent band at 1,615 cm^{-1} was attributed to C=O stretching of the amide group, while 1,580 cm^{-1} corresponded to aromatic C=C stretching. Absorptions at 1,452–1,352 cm^{-1} correlate with the C–N stretching of the indole and acridine moieties. The peak at 1,238–1,026 cm^{-1} was ascribed to C–O–C and C–N vibrational modes. The area 918–768 cm^{-1} exhibited out-of-plane C–H bending of the indole and acridine aromatic rings, corroborating the hypothesized structure.

*N-(acridin-9-yl)-2-(ethyl(o-tolyl)amino)acetamide **(AAM3)***

Chemical formula: $C_{24}H_{23}N_3O$; M.P.: 163-166 °C; Rf value: 0.89; % yield: 68. Molecular weight: 369.47 g/mol; m/z: 369.18 (100.0%), 370.19 (26.0%), 371.19 (3.2%), 370.18 (1.1%). Elemental analysis (calculated): C, 78.02; H, 6.27; N, 11.37; and O = 4.33. ^{1}H-NMR (500 MHz, DMSO) δ 9.82 (s, 1H), 8.20 – 8.05 (m, 2H), 7.62 – 7.57 (m, 2H), 7.56 – 7.41 (m, 2H), 7.41 – 7.37 (m, 2H), 7.05 – 6.95 (m, 3H), 6.70 (d, J = 20.5 Hz, 2H), 4.70 (s, 1H), 3.79 (s, 1H), 3.64 (s, 1H), 3.40 (s, 1H), 2.30 – 2.26 (m, 3H), and 1.26 – 1.22 (m, 3H). ^{13}C-NMR (126 MHz, DMSO) δ 170.31, 129.99, 129.36, 129.30, 128.79, 128.02, 127.88, 127.26, 127.02, 126.63, 67.61, and 64.87. The FTIR spectra of AAM3 exhibited a wide absorption band at 3,353 cm^{-1}, indicative of N–H stretching vibrations associated with the secondary amide group. A peak at 2,986 cm^{-1} indicated aliphatic C–H stretching. The prominent absorption bands at 1,655 cm^{-1} and 1,585 cm^{-1} are attributed to C=O (amide carbonyl) stretching and aromatic C=C stretching, respectively. The peaks at 1,455–1,372 cm^{-1} were ascribed to C–N stretching and CH_3 bending vibrations originating from the ethyl-tolyl substituent. Supplementary peaks in the 850–750 cm^{-1} range signified aromatic C–H out-of-plane bending vibrations, thus corroborating the acridine aromatic structure.

*N-(acridin-9-yl)-2-(4-oxopiperidin-1-yl)acetamide **(AC1)***

Chemical formula: $C_{20}H_{19}N_3O_2$; M.P.: 143-145 °C; Rf: 0.98; % yield: 90%. Molecular weight: 333.39 g/mol; m/z: 333.15 (100.0%), 334.15 (21.6%), 335.15 (2.2%), and 334.14 (1.1%). Elemental analysis (calculated): C, 72.05; H, 5.74; N, 12.60; and O = 9.60. ^{1}H-NMR (500 MHz, DMSO) δ 10.04 – 7.77 (m, 2H), 8.90 – 7.53 (m, 6H), 7.74 (dd, J = 7.5, 1.5 Hz, 2H), 7.47 (td, J = 7.5, 1.4 Hz, 2H), 7.21 (s, 1H), 3.27 – 3.23 (m, 2H), 3.04 – 2.85 (m, 2H), and 2.85 – 2.68 (m, 6H). ^{13}C-NMR (126 MHz, DMSO) δ 170.30, 155.81, 154.37, 129.99, 129.31, 128.03, 127.26, 127.03, 108.41, 64.86, 37.10, and 35.97. The AC1 spectra exhibited a moderate-intensity band at 3,035 cm^{-1}, indicative of aromatic C–H stretching. A prominent band at 1,596 cm^{-1} signified C=O stretching of the amide group, while 1,551 cm^{-1} corresponded to N–H bending. The bands at 1,473–1,371 cm^{-1} verified the C–N stretching of the amide and piperidine moieties. The distinctive absorptions at 1,255–998 cm^{-1} correspond to the C–O–C and C–N vibrations of the cyclic piperidinone structure. Peaks in the 897–694 cm^{-1} range resulted from aromatic C–H out-of-plane bending, confirming replacement within the acridine ring system.

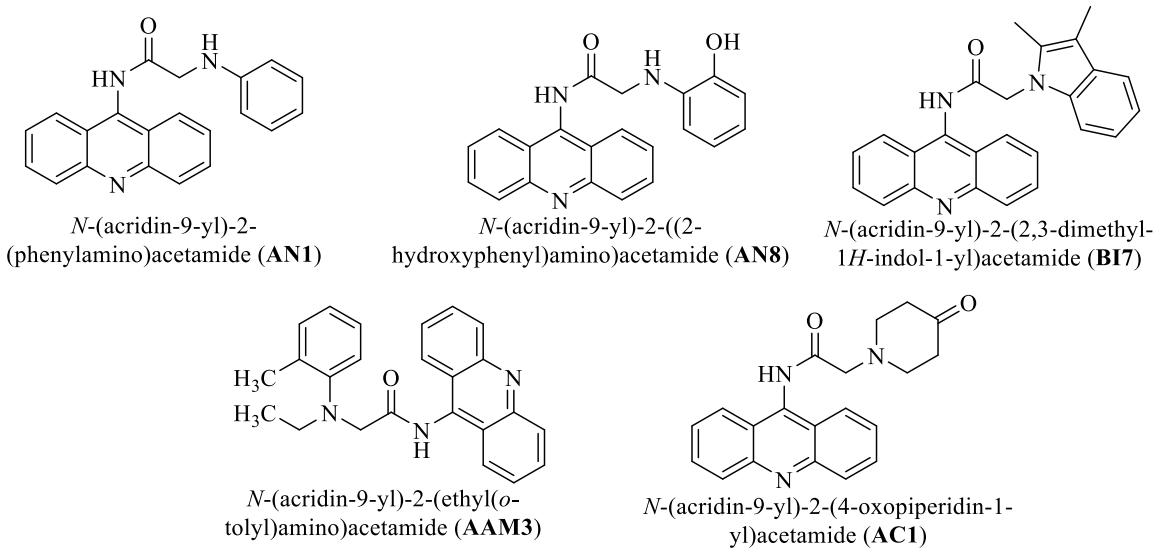

Figure 2. Chemical structures of the synthesized compounds.

Molecular docking studies

Molecular docking experiments were conducted to examine the binding between ligands and the target enzyme acetylcholinesterase (AChE). The crystal structure of human acetylcholinesterase (PDB ID: 4EY6, resolution 1.9 Å) was obtained from the Protein Data Bank. The protein structure was generated by eliminating all crystallographic water molecules, co-crystallized ligands, and heteroatoms that were not associated with the binding site. Hydrogen atoms were included to stabilize the protein structure, and energy minimization was performed using the Swiss PDB Viewer (SPDBV) with the GROMOS96 force field, guaranteeing the appropriate geometry and conformational stability of the protein [19,26]. The quality and stereochemical integrity of the minimized protein were validated using a Ramachandran plot, which confirmed that the majority of the residues were in the allowed regions, indicating a reliable structural model.

The binding pocket and active site residues of AChE were identified using a Protein-Ligand Interaction Profiler (PLIP), which provided key information about hydrogen bonding, hydrophobic interactions, and π–πstacking regions within the active cavity. The selected active site residues were cross-verified with literature reports to confirm the reliability of the predicted binding cavity. Ligands were designed and sketched using the Marvin Sketch software, and their structural integrity was checked for valence and stereochemical correctness. The ligand molecules were then converted into 3D conformations, and the energy was minimized using the MMFF94 force field to achieve low-energy, stable geometries. The optimized ligands were saved in the PDB format for further docking analysis [27–29].

Docking simulations were performed using PyRx 0.9 (AutoDock Vina engine). The grid box was delineated to include active site residues, ensuring the complete coverage of the binding pocket. Default settings were used for docking, and exhaustiveness was elevated to enhance precision. Many binding poses were produced for each ligand, and the conformation exhibiting the lowest binding energy (kcal/mol) was deemed the most advantageous binding configuration. The docking poses were further visualized and analyzed using Discovery Studio Visualizer to obtain a clear understanding of ligand orientation and specific protein–ligand interactions [19–21]. The binding energy values obtained from docking

were compared among the ligands to assess their relative affinities toward AChE, and potential structure–activity relationships were inferred. A 3D ribbon view of the target enzyme is shown in Figure 3.

MTT assay for cell viability

Cell culture

The SH-SY5Y neuroblastoma cell line was procured from Sigma-Aldrich (USA) and grown in Dulbecco's Modified Eagle's Medium (DMEM) supplemented with 10% fetal bovine serum (FBS) and growth supplements. The cells were preserved in a humidified incubator maintained at 37 °C with 5% CO_2 to replicate physiological conditions. The experimental techniques began after the cells reached approximately 80% confluence, ensuring consistency and repeatability in subsequent experiments.

Determination of cell viability

Cell viability was evaluated using the MTT reduction assay, with slight modifications, and all experiments were performed in triplicate. SH-SY5Y neuroblastoma cells (2.0×10^4/well) were seeded in 96-well plates with 100 µL of DMEM containing 10% FBS and incubated for 24 h for adhesion. Cells were then pretreated with five concentrations of test chemicals (25, 50, 100, 250, 500 µg/mL in DMEM + 10% FBS) for 2 h, followed by exposure to 10 µM $A\beta_{25-35}$ for 24 h at 37 °C with 5% CO_2. The solvent control (DMEM + 10% FBS) was maintained under identical conditions.

After treatment, the medium was replaced with 100 µL of MTT solution (500 µg/mL in PBS) and incubated for 4 h at 37 °C. The solution was then removed and the formazan crystals were solubilized with 100 µL of DMSO under gentle shaking. The absorbance was recorded at 540 nm using a microplate reader (Thermo Fisher Scientific). Cell viability was expressed as a percentage of the untreated control, indicating cytoprotective or cytotoxic effects of the test chemicals.

Preparation of test compound stock and working solutions

Stock solutions of the synthesized test compounds (4.0×10 µg/mL) were prepared in an alcohol/DMEM mixture (70:30, v/v), sterilized by filtration through a 0.22 µm membrane filter, and stored at 4 °C until further use. Working solutions (4.0×10^3 µg/mL) were freshly prepared by diluting the stock solution in complete cell culture medium before the experiments.

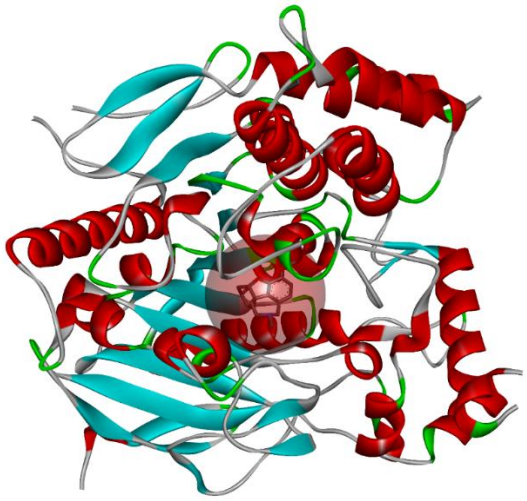

Figure 3. 3D ribbon view of the targeted enzyme with active cavity.

Preparation of $A\beta_{25-35}$ stock and working solutions

$A\beta_{25-35}$ peptide was solubilized in sterile distilled water to create a 1 mM stock solution, which was thereafter kept at −20 °C. The stock for cell treatment was diluted in DMEM with 10% FBS to provide a 100 µM working solution, resulting in a final concentration of 10 µM per sample.

Statistical analysis

All experimental procedures were conducted in triplicate to ensure the reproducibility and reliability of the findings. The obtained values are presented as mean ± standard deviation (SD). For statistical evaluation, ANOVA was employed, followed by Tukey's multiple comparison post-hoc test to determine pairwise differences among the treatment groups [30,31]. A probability level of $p < 0.05$ was considered to indicate statistical significance. All statistical analyses and graphical representations of the data were performed using the GraphPad Prism software (version X; GraphPad Software, San Diego, CA, USA).

Results and Discussion

Molecular docking studies

Molecular docking experiments were conducted to clarify the binding interactions of the produced acridine derivatives with the active site of AChE (PDB ID: 4EY6). All compounds exhibited good binding affinities, with docking scores between −8.0 and −8.3 kcal/mol, signifying robust and persistent interactions with the catalytic residues of AChE. The binding patterns indicated the participation of numerous hydrogen bonds, hydrophobic interactions, and π–π interactions, which enhanced the stability of the protein–ligand complexes.

AC1 was identified as the most promising contender, with the highest binding affinity (−8.3 kcal/mol). The binding mode revealed strong hydrogen-bonding interactions with Gly437 and Arg434, stabilizing the ligand in the catalytic groove. In addition, π–π stacking with Trp441 and Trp754, along with hydrophobic interactions involving Ala753 and Met758, enhanced the affinity of AC1 for AChE. These interactions explain the superior cytotoxicity observed experimentally, highlighting AC1 as a lead scaffold for further development.

AN1 exhibited a binding affinity of −8.1 kcal/mol and was stabilized by π-cation interactions with Lys751 and Lys587, as well as hydrogen bonding with Asn722. Hydrophobic contact with Lys436 and Pro431 further contributed to complex stabilization. However, the presence of an unfavorable donor–donor interaction with Asn722 slightly reduced the binding efficiency compared to that of AC1.

AN8 showed a docking score of −8.0 kcal/mol. The presence of the hydroxyl substituent facilitated hydrogen bonding with Lys443, while π-cation interactions with Lys439 and Arg590 contributed significantly to its binding affinity. Additional hydrophobic contacts with Lys387 and Thr591 supported the stability of the complex. The presence of both polar and hydrophobic interactions suggests that AN8 fits well with the AChE active site.

AAM3, with a docking score of −8.0 kcal/mol, exhibits multiple π–alkyl interactions with Ala625, Leu629, and Ile628, as well as π–π stacking with Tyr537. These interactions are complemented by van der Waals interactions with Asn539 and Tyr538, contributing to the stabilization of the complex. These interactions indicate that AAM3 occupies a more hydrophobic pocket of AChE, consistent with its bulky ethyltolyl substituent.

BI7 also achieved a docking score of −8.0 kcal/mol and exhibited a different binding pattern. The ligand formed π-alkyl interactions with Ala625, Ile628, Leu629, and Tyr537, while van der Waals interactions with Asn539 and Tyr538 contributed to complex stability. The presence of the indole moiety allows favorable

stacking interactions, suggesting that BI7 aligns parallel to the aromatic residues within the catalytic site.

Overall, docking analysis revealed that all compounds shared a conserved mode of binding, engaging both polar and hydrophobic residues within the AChE active pocket. Among them, AC1 displayed the strongest interactions and highest docking score (–8.3 kcal/mol), which correlates with its superior cytotoxic performance observed experimentally. These results indicate that AC1 may be a good candidate for future preclinical investigations, whereas AN1, AN8, AAM3, and BI7 provide useful structural insights for the rational design of new acridine-based AChE inhibitors. Figure 4 shows the binding postures of the compounds.

MTT assay for cell viability

The cytotoxic activity of the synthesized acridine derivatives (AN1, AN8, BI7, AAM3, and AC1) was evaluated against human SH-SY5Y neuroblastoma cells using an MTT assay. The IC_{50} values, which indicate the concentration required to reduce cell viability by 50%, revealed significant variation in the potency of the compounds (Table 1).

Among the tested molecules, AC1 exhibited the highest cytotoxic activity with an IC_{50} value of 26.92 ± 0.57 µg/mL, suggesting its strong antiproliferative potential. This superior effect correlates with its favorable docking score (–8.3 kcal/mol), indicating that the enhanced binding interactions with acetylcholinesterase may contribute to its cytotoxic response. The presence of the oxopiperidine substituent likely improved the binding affinity and promoted better cellular uptake, thereby enhancing the biological activity.

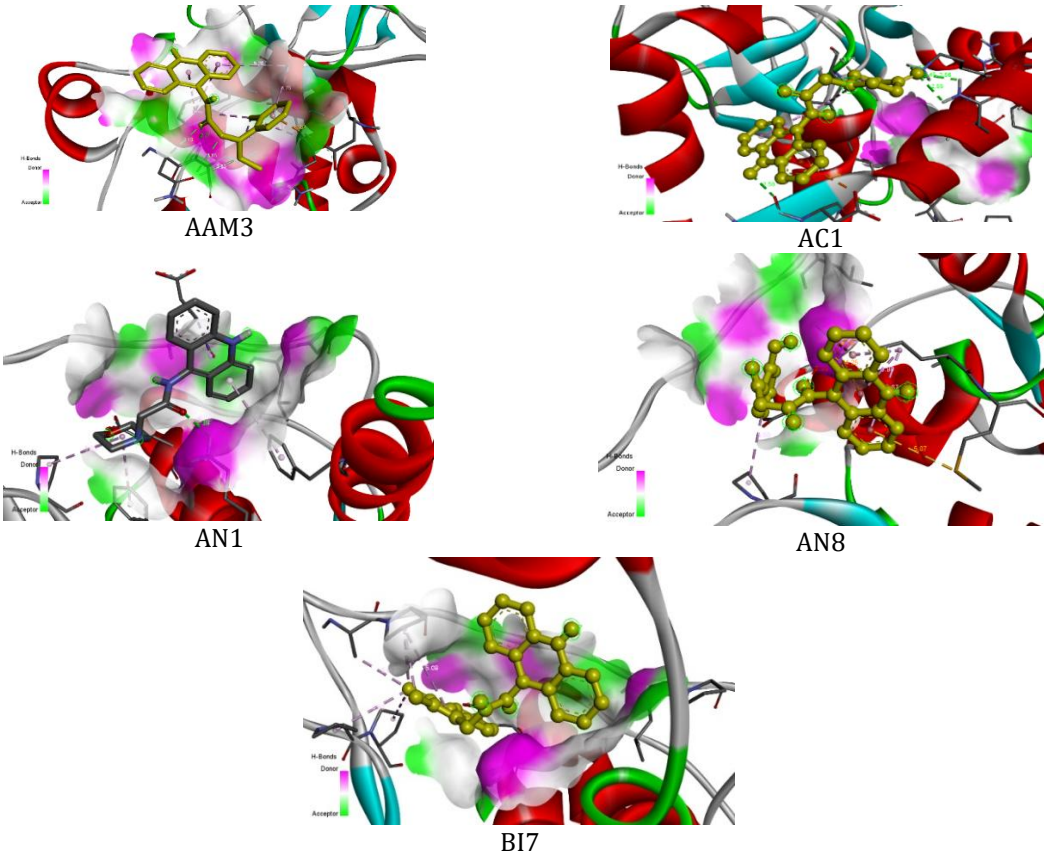

Figure 4. Predicted binding poses of synthesized acridine derivatives within the active cavity of AChE (PDB ID: 4EY6).

AN1 also demonstrated strong cytotoxicity with an IC_{50} of 47.74 ± 0.98 µg/mL. This compound formed multiple stabilizing interactions within the active site during docking and showed a docking score of –8.1 kcal/mol, consistent with its effective cell growth inhibition. The phenylamino substituent at the acetamide position may play a role in its activity through π-cation and hydrophobic interactions.

AN8 displayed moderate cytotoxicity, with an IC_{50} of 69.95 ± 0.49 µg/mL. While docking studies indicated favorable binding (–8.0 kcal/mol), its biological activity was comparatively weaker than that of AC1 and AN1. This may be due to steric hindrance or limited cellular permeability conferred by the hydroxyl group, which, while beneficial for hydrogen bonding, may reduce lipophilicity and cell membrane penetration.

In contrast, BI7 and AAM3 showed considerably weaker cytotoxic activities, with IC_{50} values of 277.19 ± 0.48 µg/mL and 279.64 ± 0.55 µg/mL, respectively. Despite docking scores comparable to those of other derivatives (–8.0 kcal/mol), these compounds failed to translate binding affinity into significant cytotoxicity. The bulky substituents in BI7 (indole moiety) and AAM3 (ethyltolyl group) may have interfered with efficient cell penetration or reduced effective intracellular concentrations, leading to lower biological activity. When compared with the standard control (IC_{50} = 92.67 ± 0.43 µg/mL), both AC1 and AN1 outperformed the reference, indicating their potential as lead scaffolds for anticancer development. The observed correlation between docking scores and *in vitro* results, particularly for AC1, reinforces the predictive value of computational modeling for identifying promising candidates.

Overall, these findings highlight that structural modifications around the acridine core significantly influence cytotoxic potential. AC1 emerged as the most potent derivative, followed by AN1, while BI7 and AAM3 were the least effective. Combined computational and experimental evidence suggests that AC1 warrants further investigation as a lead compound in preclinical studies. The IC_{50} values of these compounds are listed in Table 1.

Morphological assessment

The cytotoxic effects of the synthesized acridine derivatives (AN1, AN8, BI7, AAM3, and AC1) were evaluated against SH-SY5Y neuroblastoma cells using the MTT assay and supported by morphological analysis at graded concentrations (50, 100, 200, and 400 µg/mL; Table 2). Microscopic observations further corroborated the dose-dependent cytotoxic effects. At 50 µg/mL, AC1 induced visible morphological alterations, with cells showing shrinkage, rounding, and partial detachment, whereas AN1 and AN8 produced moderate changes. BI7 and AAM3 exhibited minimal effects at this concentration. At 100 µg/mL, cytotoxicity became more evident: AC1 disrupted the monolayer extensively, AN1 caused a notable loss of cell adherence, and AN8 induced moderate cell death, whereas BI7 and AAM3 still maintained a significant proportion of viable cells.

Table 1. Effect of compound acridine derivatives on cell viability in cultured SHSY5Y cells

Synthesised compounds	Test concentration_(µg/mL)				IC_{50}_value µg/mL
	50	100	200	400	
AN1	**63.2**	**51.74**	**48.68**	**19.58**	47.74 ± 0.98
AN8	50.28	44.71	38.74	21.54	69.95 ± 0.49
B17	45.77	41.69	36.58	29.20	277.19 ± 0.48
AAM3	60.6	60.1	60.1	75.7	279.64 ± 0.55
AC1	83.6	36.1	41.9	20.4	26.92 ± 0.57
STD	-63.9	-67.2	-61.6	-52.0	92.67 ± 0.43

These effects were more pronounced at higher concentrations. At 200 µg/mL, AC1 almost completely disrupted the cell monolayer integrity, with very few viable cells remaining. AN1 also showed strong cytotoxic effects, whereas AN8 produced moderate changes, with a partial reduction in viable cell density. BI7 and AAM3 exhibited relatively weak cytotoxicity at this dose, which is consistent with their high IC_{50} values. At 400 µg/mL, AC1 nearly eradicated the cell population, confirming its strong anti-proliferative effect. AN1 also induced extensive cell death, while AN8 produced substantial cytotoxicity, although less intense than AC1 and AN1. BI7 and AAM3 remained less effective, with scattered viable cells still visible even at high concentrations. Morphological changes observed at different concentrations are presented in Table 2.

Table 2. Morphological changes in SH-SY5Y cells treated with acridine derivatives

50_µg/mL	100_µg/mL	200_µg/mL	400_µg/mL
AN1			
			
AAM5			
	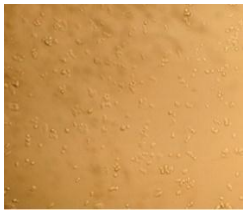		
AC1			
	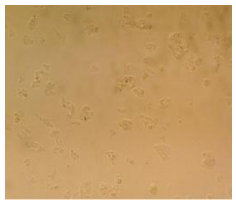	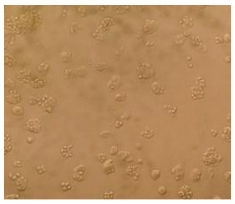	
AN8			
	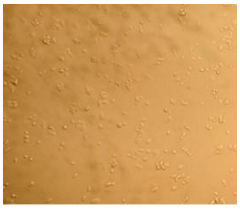		
BI7			
			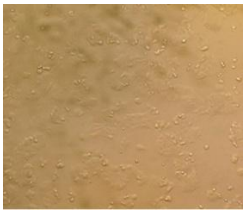

Taken together, both the quantitative and qualitative analyses demonstrated a strong dose-dependent cytotoxic response. AC1 consistently emerged as the most potent derivative, followed by AN1 and AN8, whereas BI7 and AAM3 were significantly less effective. These findings are in agreement with the molecular docking results, where AC1 showed the best binding affinity (–8.3 kcal/mol) through multiple stabilizing interactions with acetylcholinesterase active site residues. Combined computational and experimental data suggest that structural modifications at the aminoacetamide position of the acridine nucleus critically influence cytotoxic potential, with the oxopiperidine-substituted derivative AC1 identified as a promising lead candidate for further preclinical development.

Conclusion

This work includes the synthesis, characterization, and evaluation of a novel series of acridine-based aminoacetamide derivatives using molecular docking and *in vitro* cytotoxicity assays. All compounds had advantageous binding affinities for AChE, facilitated by robust hydrogen bonding, hydrophobic interactions, and π–π stacking interactions. Among them, AC1 emerged as the most potent derivative, showing the strongest docking score (–8.3 kcal/mol) and the lowest IC_{50} value (26.92 ± 0.57 µg/mL) against SH-SY5Y neuroblastoma cells. AN1 also showed notable activity, whereas BI7 and AAM3 were less effective. The strong correlation between docking predictions and cytotoxicity outcomes highlights the utility of computational approaches for guiding experimental drug discovery. Structural modifications at the aminoacetamide position of acridine significantly modulate biological activity, underscoring the importance of rational design. Overall, this study identified acridine-based aminoacetamide derivatives, particularly AC1, as promising scaffolds for anticancer therapy. These results justify further *in vivo* efficacy and toxicity studies to advance the use of AC1 as a preclinical candidate.

Disclosure Statement

No potential conflicts of interest were reported by the authors in this work.

ORCID

Joel Mart E.: 0009-0000-9560-674X
Ronald Darwin Chellappan: 0000-0002-2731-8196

References

[1] Kothamunireddy, V.D., Galla, R. Synthesis, characterization and biological evaluation of novel acridine derivatives for anti-inflammatory and analgesic activities. *Indian Journal of Pharmaceutical Sciences*, **2021**, 83(5), 1016–23.
[2] Sondhi, S.M., Singh, J., Rani, R., Gupta, P., Agrawal, S., Saxena, A. Synthesis, anti-inflammatory and anticancer activity evaluation of some novel acridine derivatives. *European Journal of Medicinal Chemistry*, **2010**, 45(2), 555–563.
[3] Sondhi, S.M., Bhattacharjee, G., Jameel, R.K., Shukla, R., Raghubir, R., Lozach, O., Meijer, L. Antiinflammatory, analgesic and kinase inhibition activities of some acridine derivatives. *Central European Journal of Chemistry*, **2004**, 2(1), 1–15.
[4] Nguyen, V.T., Haug, G.C., Nguyen, V.D., Vuong, N.T., Karki, G.B., Arman, H.D., Larionov, O.V. Functional group divergence and the structural basis of acridine photocatalysis revealed by direct decarboxysulfonylation. *Chemical Science*, **2022**, 13(14), 4170–4179.
[5] Kar, S., Milstein, D. Sustainable catalysis with fluxional acridine-based PNP pincer complexes. *Chemical Communications*, **2022**, 58(23), 3731–3746.
[6] Nafisi, S., Saboury, A.A., Keramat, N., Neault, J.-F., Tajmir-Riahi, H.-A. Stability and structural features of DNA intercalation with ethidium bromide, acridine orange and methylene blue. *Journal of Molecular Structure*, **2007**, 827(1-3), 35–43.
[7] Makhaeva, G.F., Lushchekina, S.V., Boltneva, N.P., Serebryakova, O.G., Rudakova, E.V., Ustyugov, A.A., Bachurin, S.O., Shchepochkin, A.V., Chupakhin, O.N., Charushin, V.N. 9-substituted acridine derivatives as acetylcholinesterase and butyrylcholinesterase inhibitors possessing antioxidant activity for

alzheimer's disease treatment. *Bioorganic & Medicinal Chemistry*, **2017**, 25(21), 5981–5994.
[8] Elmusa, M., Elmusa, S., Mert, S., Kasımoğulları, R., Türkan, F., Atalar, M.N., Bursal, E. One-pot three-component synthesis of novel pyrazolo-acridine derivatives and assessment of their acetylcholinesterase inhibitory properties: An *in vitro* and *in silico* study. *Journal of Molecular Structure*, **2023**, 1274, 134553.
[9] Makhaeva, G.F., Kovaleva, N.V., Rudakova, E.V., Boltneva, N.P., Lushchekina, S.V., Astakhova, T.Y., Timokhina, E.N., Serebryakova, O.G., Shchepochkin, A.V., Averkov, M.A. Derivatives of 9-phosphorylated acridine as butyrylcholinesterase inhibitors with antioxidant activity and the ability to inhibit β-amyloid self-aggregation: Potential therapeutic agents for alzheimer's disease. *Frontiers in pharmacology*, **2023**, 14, 1219980.
[10] Walczak-Nowicka, Ł.J., Herbet, M. Acetylcholinesterase inhibitors in the treatment of neurodegenerative diseases and the role of acetylcholinesterase in their pathogenesis. *International Journal of Molecular Sciences*, **2021**, 22(17), 9290.
[11] Shoukat, S., Zia, M.A., Uzair, M., Attia, K.A., Abushady, A.M., Fiaz, S., Ali, S., Yang, S.H., Ali, G.M. Bacopa monnieri: A promising herbal approach for neurodegenerative disease treatment supported by in silico and *in vitro* research. *Heliyon*, **2023**, 9(11), e21161.
[12] Scarpini E, Scheltens P, Feldman H. Treatment of alzheimer's disease: Current status and new perspectives. *The Lancet Neurology*. **2003**, 2(9), 539–547.
[13] Goni, L.K., Jafar Mazumder, M.A., Tripathy, D.B., Quraishi, M.A. Acridine and its derivatives: Synthesis, biological, and anticorrosion properties. *Materials*, **2022**, 15(21), 7560.
[14] Varakumar, P., Rajagopal, K., Aparna, B., Raman, K., Byran, G., Gonçalves Lima, C.M., Rashid, S., Nafady, M.H., Emran, T.B., Wybraniec, S. Acridine as an anti-tumour agent: A critical review. *Molecules*, **2022**, 28(1), 193.
[15] Huo, L., Liu, X., Jaiswal, Y., Xu, H., Chen, R., Lu, R., Nong, Y., Williams, L., Liang, Y., Jia, Z. Design and synthesis of acridine-triazole and acridine-thiadiazole derivatives and their inhibitory effect against cancer cells. *International Journal of Molecular Sciences*, **2022**, 24(1), 64.
[16] Klimaeva LA, Klochneva MA. The study of kinetic parameters of the hydrogen evolution reaction in the presence of acridine and its derivatives. *Bulletin of Perm University. Chemistry Series*, **2022**, 12, 52–9.
[17] Feng, Y.S., Ma, J.J., Lin, X.Y., Zhang, J.S., Lv, P., Xu, H.J., Luo, L.B. Covalent functionalization of graphene oxide by 9-(4-aminophenyl) acridine and its derivatives. *Chinese Chemical Letters*, **2012**, 23(12), 1411–1414.
[18] Byvaltsev, V.A., Bardonova, L.A., Onaka, N.R., Polkin, R.A., Ochkal, S.V., Shepelev, V.V., Aliyev, M.A., Potapov, A.A. Acridine orange: A review of novel applications for surgical cancer imaging and therapy. *Frontiers in Oncology*, **2019**, 9, 925.
[19] Siddiqui, F., Makhloufi, R., Salah, M.E.-S., Mohamed, E., Hojjati, M. Computational exploration of quinine and mefloquine as potential anti-malarial agents. *Journal of Pharmaceutical Sciences and Computational Chemistry*, **2025**, 1(2), 106–115.
[20] Ahmed, S., Tabassum, P., Falak, S., Ahmad, A., Shaikh, M. Molecular docking and network pharmacology: Investigating vitis vinifera phytoconstituents as multi-target therapeutic agents against breast cancer. *Journal of Pharmaceutical Sciences and Computational Chemistry*, **2025**, 1(2), 116–134.
[21] Jadhav, S., Dighe, P. Synthesis, In vitro evaluation, and molecular docking studies of novel pyrazoline derivatives as promising bioactive molecules. *Journal of Pharmaceutical Sciences and Computational Chemistry*, **2025**, 1(3), 190–209.
[22] Daud, H., Ghani, A., Iqbal, D.N., Ahmad, N., Nazir, S., Muhammad, M.J., Hussain, E.A., Nazir, A., Iqbal, M. Preparation and characterization of guar gum based biopolymeric hydrogels for controlled release of antihypertensive drug. *Arabian Journal of Chemistry*, **2021**, 14(5), 103111.
[23] Bukhary, S.K.H.S., Choudhary, F.K., Iqbal, D.N., Ali, Z., Sadiqa, A., Latif, S., Al-Ahmary, K.M., Basheer, S., Ali, I., Ahmed, M. Development and characterization of a biodegradable film based on guar gum-gelatin@ sodium alginate for a sustainable environment. *RSC Advances*, **2024**, 14(27), 19349–19361.
[24] Sundarajan, S., Abdurahman, N.H. Chemical compound characterizations of patchouli leaf extract via GC-MS, LC-QTOF-MS, FTIR, and 1H NMR. *International Journal of Engineering Research & Technology*, **2019**, 8(6), 1054–1059.
[25] Dybowski, M.P., Holowinski, P., Typek, R., Dawidowicz, A.L. Comprehensive analytical and structural characteristics of methyl 3, 3-dimethyl-2-(1-(pent-4-en-1-yl)-1H-indazole-3-carboxamido) butanoate (MDMB-4en-PINACA). *Forensic Toxicology*, **2021**, 39(2), 481–492.
[26] Tamboli, A., Tayade, S. In-depth investigation of berberine and tropane through computational screening as possible DPP-IV inhibitors for the treatment of T2DM. *Journal of Pharmaceutical Sciences and Computational Chemistry*, **2025**, 1(1), 1–11.

[27] Khan, S.L., Bakshi, V. LC-HRMS and *in silico* analysis of ailanthus excelsa metabolites targeting EGFR triple mutation (L858R/T790M/C797S). *Advanced Journal of Chemistry, Section A,* **2026**, 9(2), 292–311.

[28] Prathyusha S, Shankar Gupta P, Kumar AK, Hussain Syed S, Shaik M, Jahnavi P, Rani S, Rajashakar V. Theoretical and computational study of bioactive compounds from myrica nagi as inhibitors of neuroendocrine and opioid receptors: A molecular docking and dynamics approach. *Advanced Journal of Chemistry, Section A,* **2026**, 9(2), 223–42.

[29] Kale, M., Wayal, S. Molecular docking, synthesis and biological screening of some novel benzothiazoles as acetylcholinesterase inhibitors. *Advanced Journal of Chemistry, Section A*, **2026**, 9(2), 208–222.

[30] Yu, Z., Guindani, M., Grieco, S.F., Chen, L., Holmes, T.C., Xu, X. Beyond t test and ANOVA: Applications of mixed-effects models for more rigorous statistical analysis in neuroscience research. *Neuron*, **2022**, 110(1), 21–35.

[31] Chen, W.-H., Uribe, M.C., Kwon, E.E., Lin, K.-Y.A., Park, Y.-K., Ding, L., Saw, L.H. A comprehensive review of thermoelectric generation optimization by statistical approach: Taguchi method, analysis of variance (ANOVA), and response surface methodology (RSM). *Renewable and sustainable energy reviews*, **2022**, 169, 112917.

HOW TO CITE THIS ARTICLE

J. Mart E., R. Darwin Chellappan. Design, Synthesis, Molecular Docking, and Cytotoxic Evaluation of Novel Acridine-Based Aminoacetamide Derivatives as Potential Acetylcholinesterase Inhibitors. *Adv. J. Chem. A*, 2026, 9(4), 739-753.

DOI: 10.48309/AJCA.2026.546506.1924
URL: https://www.ajchem-a.com/article_235452.html